한국소음진동공학회 창립10주년 기념 소음진동학술대회논문집, pp. 724~730.

연속웨이블렛 변환의 활용에 대한 이론적 배경

김윤영*, 김응훈**

Theoretical Background for the Application of the Continuous Wavelet Transform

Yoon Young Kim, Eung-Hun Kim

ABSTRACT

Although there have been many investigations employing the continuous wavelet transform for the analysis of dispersive waves, they seem to lack theoretical justifications for the effectiveness of the continuous wavelet transform over other time-frequency analysis tools such as the short-time Fourier transform. The goal of this paper is to answer this question by investigating theoretically the performance of the continuous wavelet transform and the short-time Fourier transform in tracing rapidly time-varying flexural waves. As a specific example, the performance of the two transforms is compared in a problem dealing with flexural waves generated by an impact in a solid circular cylinder.

1. TIME-FREQUENCY ANALYSIS : CWT VS STFT

1.1 Short Time Fourier Transform (STFT)

The short-time Fourier transform of a function f belonging to a finite-energy signal space $L^2(t)$ is defined as (see Mallat [1])

$$\begin{aligned} Sf(u,\xi) &= \int_{-\infty}^{+\infty} f(t) g^*_{u,\xi}(t) dt \\ &= \int_{-\infty}^{+\infty} f(t) g(t-u) e^{-i\xi t} dt \end{aligned} \tag{1}$$

with

$$g_{u,\xi}(t) = e^{i\xi t} g(t-u) \tag{2}$$

where $*$ denotes the complex conjugate. The transform $Sf(u,\xi)$ can measure the behavior of f in the neighborhood of time, u and frequency, ξ. The function $g(t)$ in Eq.(1) is the window function, which is assumed to be real and symmetric. For a given window $g(t)$ with the time spread σ_t and frequency spread σ_ω, the time and frequency spreads of the modulated translated window $g_{u,\xi}(t)$ are independent of (u,ξ). This means that the short-time Fourier transform has the same resolution across the time-frequency plane.

Mallat [1] illustrates the effectiveness of STFT in dealing with signals having slowly varying instantaneous frequencies such as linear and quadratic chirps.

The instantaneous frequency is defined as the positive derivative of $\phi(t)$

$$\omega_{\text{inst}}(t) = \frac{d\phi(t)}{dt} \tag{3}$$

where $\phi(t)$ is the modulating phase for a real signal $f(t)$ having an amplitude $a(t)$

$$f(t) = a(t) e^{i\phi(t)} \quad (a(t) \geq 0) \tag{4}$$

1.2 Continuous Wavelet Transform (CWT)

The definition of the continuous wavelet transform is

$$\begin{aligned} W_f(u,s) &= \int_{-\infty}^{+\infty} f(t) \psi^*_{u,s}(t) dt \\ &= \int_{-\infty}^{+\infty} f(t) \frac{1}{\sqrt{s}} \psi^*\left(\frac{t-u}{s}\right) dt \end{aligned} \tag{5}$$

with

$$\psi_{u,s}(t) = \frac{1}{\sqrt{s}} \psi\left(\frac{t-u}{s}\right) \tag{6}$$

The function $\psi(t)$ is called a mother wavelet satisfying the admissibility condition (see Mallat [1])

$$\int_{-\infty}^{+\infty} \frac{|\hat{\psi}(\omega)|^2}{|\omega|} d\omega < \infty \tag{7}$$

* 정회원, 서울대학교 기계항공공학부

** 서울대학교 정밀기계설계 공동연구소

where $\hat{\psi}(\omega)$ is the Fourier transform of $\psi(t)$.

The existence of the integral in Eq.(7) requires that

$$\hat{\psi}(0) = 0 \tag{8}$$

In order to see the advantage of WT over STFT, we need to examine the tiling of WT in the time-frequency plane. To this end, we assume that the center frequency of $\hat{\psi}(\omega)$ is η and that the time and frequency spreads of $\psi(t)$ are σ_t and σ_ω, respectively. Since $\psi_{u,s}(t)$ involves scaling by s, we can show that the time and frequency spreads of $\psi_{u,s}$ are $s\sigma_t$ and σ_ω/s, respectively. We can also show that the center of the corresponding Heisenberg box is located at $(u, \eta/s)$.

The Gabor wavelet $\psi(t)$ is a complex-valued modulated Gaussian function defined as

$$\psi(t) = e^{i\eta t} g(t) \tag{9a}$$

$$g(t) = \frac{1}{(\sigma^2\pi)^{1/4}} e^{-t^2/2\sigma^2} \tag{9b}$$

where η is the center frequency of the $\hat{\psi}(\omega)$ and σ is a measure of the spread of $\psi(t)$. The shape of the Gabor wavelet is controlled by the product G_s of η and σ

$$G_s = \sigma\eta \tag{10}$$

This parameter, which may be called the Gabor shaping factor [2], affects significantly the time resolution of the wavelet and thus the performance of the corresponding wavelet transform. Although Eq. (8) requires that $G_s \to \infty$, the condition $G_s >> 1$ suffices for actual numerical computation. The Gabor wavelet satisfying this condition can be an approximate analytic wavelet. Kim and Kim [2] have reported the importance of an optimal selection of G_s in the analysis of dispersive waves. In this work, we will investigate theoretically the effect of G_s on the performance of the Gabor wavelet transform.

1.3 Ridge Method for Instantaneous Frequency Estimation

The spectrogram $P_s f(u,\xi) = |Sf(u,\xi)|^2$ and the normalized scalogram $\frac{\xi}{\eta} P_w f(u,\xi) = |W_f(u,s)|^2/s$ (with $\xi = \eta/s$) measure the energy of f in a time-frequency neighborhood of (u,ξ). The ridge algorithm [3] computes instantaneous frequencies from the local maxima of spectrogram and scalogram. The result of the ridge analysis provides criteria to select windows for STFT and mother wavelets for WT.

For the analysis, it is assumed that the signal $f(t)$ takes the following form:

$$f(t) = a(t)\cos\phi(t) \tag{11}$$

where $a(t)$ and $\phi(t)$ are an amplitude and a time-varying phase of $f(t)$. The instantaneous frequency ω_{inst} is defined by Eq.(3).

STFT

It is convenient to introduce a scaling parameter s to adjust the size of window $g(t)$ such that

$$g_{s,u,\xi}(t) = \frac{1}{\sqrt{s}} g(\frac{t-u}{s}) e^{i\xi t} \tag{12}$$

For the subsequent analysis, it is assumed that the support of a real symmetric window is $[-\frac{1}{2}, \frac{1}{2}]$, and $|\hat{g}(\omega)| \le \hat{g}(0)$ for all frequencies ω.

Using $g_{s,u,\xi}(t)$ as the windowed Fourier atom, the following result can be found

$$\begin{aligned} Sf(u,\xi) &= \int_{-\infty}^{+\infty} f(t) g^*_{s,u,\xi}(t)dt \\ &= \frac{\sqrt{s}}{2} a(u) e^{i(\phi(u)-\xi u)} (\hat{g}(s[\xi - \dot{\phi}(u)]) + \epsilon(u,\xi)) \end{aligned} \tag{13}$$

Where $\hat{\cdot}$ denotes the differentiation with respect to its own argument.

The corrective term, or the error term, $\epsilon(u,\xi)$ is bounded by

$$|\epsilon(u,\xi)| \le \epsilon_{a,1} + \epsilon_{a,2} + \epsilon_{\phi,2} + \sup_{|\omega| \ge |s\dot{\phi}(u)|} |\hat{g}(\omega)| \tag{14}$$

with

$$\epsilon_{a,1} \le \frac{s|\dot{a}(u)|}{|a(u)|} \tag{15a}$$

$$\epsilon_{a,2} \le \sup_{t \in [u-\frac{s}{2}, u+\frac{s}{2}]} \frac{s|\ddot{a}(t)|}{|a(u)|} \tag{15b}$$

If $\frac{s|\dot{a}(u)|}{|a(u)|} \le 1$, (this condition is satisfied in most engineering applications),

$$\epsilon_{\phi,2} \le \sup_{t \in [u-\frac{s}{2}, u+\frac{s}{2}]} s^2 |\ddot{\phi}(t)| \tag{16}$$

The last term in Eq. (14) can be negligible if

$$s|\dot{\phi}(u)| \ge \Delta\omega \tag{17}$$

where $\Delta\omega$ is the bandwidth of the selected window $\hat{g}(\omega)$.

At ridges, *i. e.*, at $\xi(u) = \dot{\phi}(u)$, the spectrogram $P_s(u,\xi) = |Sf(u,\xi)|^2$ becomes maximum and $\epsilon_{a,1}$ is given by

$$\epsilon_{a,1} = \frac{s|\dot{a}(u)|}{|a(u)|} |\dot{\hat{g}}(2s\dot{\phi}(u))| \tag{18}$$

This term is negligible when Eq. (17) is satisfied. Thus at ridge points

$$P_s(u,\xi) = |Sf(u,\xi)|^2 = \frac{s}{2} a^2(u) (\hat{g}(0) + \epsilon_{a,2} + \epsilon_{\phi,2})^2 \tag{19}$$

In order to extract instantaneous frequencies accurately by using the spectrogram, the following conditions must

be met:

$$\epsilon_{a,2} \leq \sup_{t\in[u-\frac{s}{2},u+\frac{s}{2}]} \frac{s|\ddot{a}(t)|}{|a(u)|} \ll 1 \tag{20a}$$

$$\epsilon_{\phi,2} \leq \sup_{t\in[u-\frac{s}{2},u+\frac{s}{2}]} s^2|\ddot{\phi}(t)| \ll 1 \tag{20b}$$

$$\frac{\Delta\omega}{s\dot{\phi}(u)} \ll 1 \tag{20c}$$

WT

As in STFT, $Wf(u,s)$ for a signal $f(t)$ given by Eq.(11) can be expressed as

$$\begin{aligned} Wf(u,s) &= \int_{-\infty}^{+\infty} f(t)\psi^*_{u,s}(t)dt \\ &= \frac{\sqrt{s}}{2}a(u)e^{i\phi(u)}(\hat{g}(s[\xi-\dot{\phi}(u)]) + \epsilon(u,\xi)) \end{aligned} \tag{21}$$

where the corrective term $\epsilon(u,\xi)$ is given by Eq.(14). Following the same treatment used for the ridge analysis of $Ws(u,\xi)$, the normalized scalogram at the ridge points, $\xi = \dot{\phi}(u)$, is given by

$$\begin{aligned} \frac{\xi}{\eta}P_w f(u,\xi) &= \frac{|W_f(u,s)|^2}{s} \\ &= \frac{1}{4}a^2(u)|\hat{g}(\eta[1-\frac{\dot{\phi}(u)}{\xi}] + e(u,\xi)|^2 \end{aligned} \tag{22}$$

where

$$s = \frac{\eta}{\xi}$$

The corrective terms $\epsilon_{a,2}$ and $\epsilon_{\phi,2}$ become negligible when

$$\frac{s^2|\ddot{a}(u)|}{|a(u)|} = \frac{\eta^2}{|\dot{\phi}(u)|^2}\frac{\ddot{a}(u)}{a(u)} \ll 1 \tag{23a}$$

$$s^2|\ddot{\phi}(u)| = \eta^2\frac{\ddot{\phi}(u)}{|\dot{\phi}(u)|^2} \ll 1 \tag{23b}$$

$$\frac{\Delta\omega}{s\phi} = \frac{\Delta\omega}{\eta} \leq 1 \tag{23c}$$

2. ANALYSIS OF NEAR-FIELD WAVES GENERATED BY AN IMPACT

In order to show the advantage of CWT over STFT, we consider a damage detection problem in which bending waves are generated by an impact. This problem was studied earlier by Kim and Kim [2].

2.1 Damage Detection Problem

Figure 1 (a) shows a simply-supported beam having a cross section. The beam is excited by a steel ball dropped at the center of the beam marked by A. The experimentally estimated duration of the contact time between the ball and the beam is to be about $85\mu sec$. Bending strains generated by the impact are measured by strain gages at the sampling rate of $1\mu sec$ at point B.

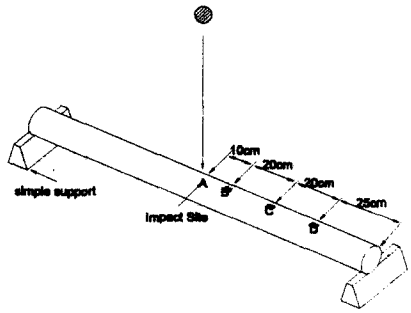

(a) Experimental setup

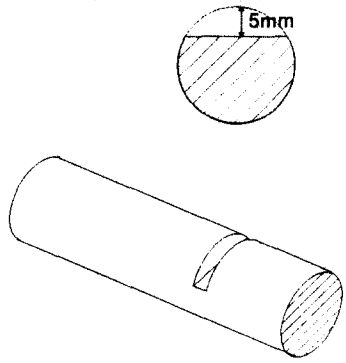

(b) Close view at C

Figure 1: Experimental setup for a solid circular beam excited by a steel ball at the center. (Diameter : $d = 2$cm, Young's modulus : $E = 117.2$GPa, Density : $\rho = 8.90 * 10^3 \mathrm{kg/m^3}$)

The beam has a small cut at location C and Fig. 1 (b) shows the shape and size of the cut. Kim and Kim [2] proposed a damage diagnostic technique based on the continuous wavelet transform and this paper gives the theoretical background for the success of the wavelet transform.

2.2 Wave Propagation In Beams

The governing wave equations by the Timoshenko beam theory are given by (see doyle [4])

$$KAG[\frac{\partial^2 v}{\partial x^2} - \frac{\partial\psi}{\partial x}] = \rho A\frac{\partial^2 v}{\partial t^2} \tag{24a}$$

$$EI\frac{\partial^2\psi}{\partial x^2} + KGA[\frac{\partial v}{\partial x} - \psi] = \rho I\frac{\partial^2\psi}{\partial t^2} \tag{24b}$$

where t and x are the time and the axial coordinate. The transverse displacement of the neutral axis and the rotation of the normal of a beam denoted by v and ψ, respectively.

Assuming the solution of Eq. (24) in propagating wave form,

$$v = v_0 e^{-i(kx-\omega t)} \tag{25a}$$

$$\phi = \phi_0 e^{-i(kx-\omega t)} \tag{25b}$$

the following dispersion relation can be found (see, e. g., Doyle [4]), which relates the wavenumber k and the frequency ω.

$$k = \pm\{\frac{1}{2}[(\frac{1}{c_s})^2 + (\frac{1}{c_b})^2]\omega^2 \pm\sqrt{(\frac{\omega}{c_b q})^2 + \frac{1}{4}[(\frac{1}{c_s})^2 - (\frac{1}{c_0})^2]^2\omega^4}\}^{1/2} \quad (26)$$

In Eq. (26), c_b, c_s and q are defined as

$$c_b \equiv \sqrt{\frac{E}{\rho}} \quad c_s \equiv \sqrt{\frac{KG}{\rho}} \quad q \equiv \sqrt{\frac{I}{A}} \quad (27)$$

The arrival time of a wave signal is governed by the group velocity C_g defined as

$$C_g \equiv \frac{d\omega}{dk} \quad (28)$$

2.3 Phase Analysis of Strain Signals

Assuming that the impact at A (see Fig. 1(a)) generates an ideal impulse, the captured signal at a location, which is L cm apart from A, can be written as

$$\epsilon^B(t) = r\frac{d\psi}{dx}|_{x=L} = -rki\psi_0 e^{-i(kx-\omega t)}|_{x=L} = rk(\omega)\psi_0 e^{-i(kL-\omega t+\frac{\pi}{2})} \quad (29)$$

where $\epsilon^B(t)$ in Eq. (29) denotes the contribution of a wave component having a circular frequency ω. Note that the magnitude ψ_0 is independent of ω since the beam is assumed to be excited by an ideal impulse. The radius of the beam is denoted by r in Eq. (29).

If the frequency of the strain signal arriving at $t = t_a$ is denoted by $\omega(t_a)$, the corresponding phase $\phi(t_a)$ and magnitude $a(t_a)$ of the strain can be written as

$$\phi(t_a) = \omega(t_a)t_a - k(\omega(t_a))L - \frac{\pi}{2} \quad (30a)$$

$$a(t_a) = rk(\omega(t_a)) \quad (30b)$$

The instantaneous frequency $d\phi(t_a)/dt_a$ of the measured strain becomes

$$\frac{d\phi(t_a)}{dt_a} = \frac{d\omega(t_a)}{dt_a}t_a + \omega(t_a) - \frac{dk}{d\omega}|_{\omega=\omega_a}\frac{d\omega(t_a)}{dt_a}L = \frac{d\omega(t_a)}{dt_a}(t_a - \frac{dk}{d\omega}|_{\omega=\omega_a}L) + \omega(t_a) \quad (31)$$

Since the arrival time of a wave component having $\omega = \omega_a$ can be expressed as

$$t_a = \frac{L}{C_g(\omega_a)} = \frac{L}{\frac{d\omega}{dk}|_{\omega=\omega_a}} = \frac{dk}{d\omega}|_{\omega=\omega_a}L \quad (32)$$

Eq. (31) can be simplified as

$$\frac{d\phi(t_a)}{dt_a} = \omega(t_a) \quad (33)$$

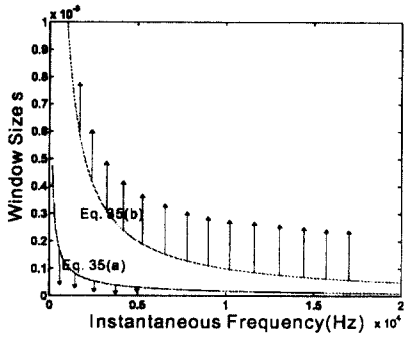

Figure 2: The allowable window size for the applicability of STFT (no window size satisfies all the nessary condition for the frequency range of interest.

Dropping the subscript a in Eq.(33), we obtain:

$$\dot{\phi}(t) = \omega(t) \quad (34a)$$

$$\ddot{\phi}(t) = \dot{\omega}(t) \quad (34b)$$

where $\omega(t)$ in Eq. (31) must be found by solving Eq.(32) for a given arrival time.

2.4 The Applicability of STFT and CWT

To investigate the applicability of STFT and CWT to the problem in consideration, it is remarked that the bending wave components are accurately measured below 30 kHz because of the excitation and measurement method. Thus we are mainly concerned with the instantaneous frequency components in the range between 5 kHz and 20 kHz.

The applicability of STFT and CWT may be assessed by examining how well the condition Eq. (20) for STFT and the condition Eq. (23) for WT are satisfied.

STFT

In order to extract the instantaneous frequency accurately from the ridges of STFT, the conditions stated by Eqs. (20) must be met. To look for the size s of a window $g(t)$, Eqs. (20) is rewritten as

$$s \ll \sqrt{\frac{1}{\ddot{\phi}(t_a)}} \quad (35a)$$

$$s \gg \frac{1}{\dot{\phi}(t_a)} \quad (35b)$$

Where the bandwidth $\Delta\omega$ of $\hat{g}(\omega)$ is assumed to be $O(1)$. (For instance, $\Delta\omega = 1.44$ for the Hanning window whose support is $[-\frac{1}{2}, \frac{1}{2}]$).

Figure 2 shows the three curves representing Eqs. (35) where the abscissa is the instantaneous frequency. It is clear that there is no window size s satisfying simultaneously the conditions given by Eqs. (35) for the frequency range of interest. As a result, STFT cannot accurately frame the time-varying instantaneous frequencies of the strain signal.

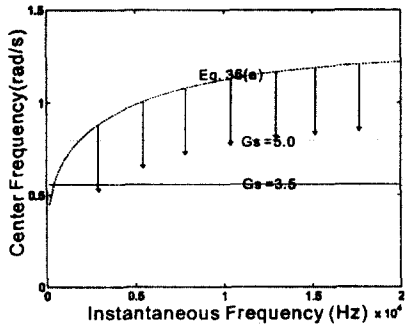

Figure 3: The allowable range of the center frequency η for CWT.

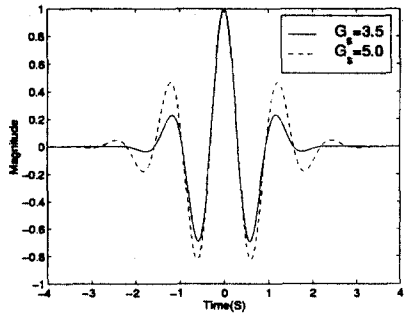

Figure 4: The real parts of the Gabor wavelets with $G_s = 3.5$ and $G_s = 5.0$(Morlet wavelet)

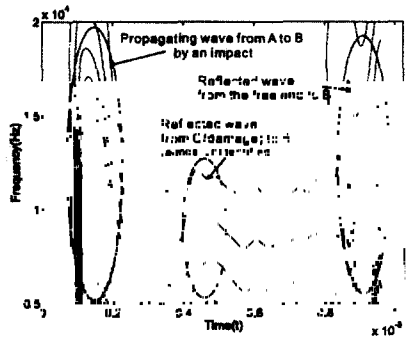

Figure 5: The spectrogram for the strain signal measured at B in a beam shown in Fig. 1. ($s = 128 \times 10^{-6}$ sec)

CWT

To obtain satisfactory results from CWT, the conditions stated by Eqs. (23) must be fulfilled. To look for the center frequency η satisfying Eqs. (23), They are rewritten as

$$\eta \ll \frac{\dot{\phi}(u)}{\sqrt{\ddot{\phi}(u)}} \tag{36a}$$

$$\eta \gg 1 \tag{36b}$$

When a Gabor wavelet is employed for CWT, we may set $\sigma = 1$ without the loss of generality and thus η is equal to G_s.

Using Eqs. (36), one can plot Fig. 3 that shows the allowable region for the center frequency η of the mother wavelet. Figure 3 clearly shows the advantage of CWT. Unlike STFT, there exists a range of η satisfying all the necessary conditions that must be satisfied for successful applications of CWT in the extraction of instantaneous frequencies. The effect of the values of G_s on the performance of CWT is clear; the smaller η is, the larger the range of instantaneous frequencies to be analyzed becomes. However, G_s must be sufficiently large enough not to violate the admissibility condition by Eq. (7). The minimum numerical value of G_s that satisfies the admissibility condition is approximately 3.5.

Figure 4 compares the real parts of the Gabor wavelets with $G_s = 3.5$ and $G_s = 5.0$. The shorter time support for $G_s = 3.5$ is advantageous for better time localization. The effective support of the Gabor wavelet is taken as $[-4, 4]$ for actual numerical implementation.

Most existing investigations have used the Morlet wavelet which is the Gabor wavelet with $G_s = 5.0$ (see, e. g., Hamada [5], et al., Inoue, et al. [6]). However, Kim and Kim [2] have recently applied the Gabor wavelet with $G_s = 3.5$ for damage detection and illustrated the advantage of using a smaller value of G_s.

2.5 Experimental Verification

To test the performance of STFT and CWT, the near-field signal measured at location B (see Fig. 1) is analyzed by STFT and CWT. The beam in consideration has a small cut at C.

Figure 5 shows the spectrogram with $s = 128 \times 10^{-6}$. Because the conditions stated by Eq. (35) is not simultaneously satisfied with any value of the window size s, It is difficult to extract instantaneous frequency information accurately from the result by STFT. In particular, it is almost impossible to tell the presence of the damage from the spectrogram.

On the other hand, the application of CWT to the same signal gives quite satisfactory results: see Fig. 6 and Fig. 7. It is clear that the reflected wave from the damaged location B where magnitude is quite small can be now detected by CWT. Although CWT with $G_s = 5.0$ can capture the reflected wave from the damage, it is obvious that CWT with $G_s = 3.5$ captures the reflected wave more accurately. To see the effect of the value of G_s (or η) on the analysis accuracy, we compare the predicted distances from B to the damage location C in Fig. 7.

In order to estimate the distance d, we used

$$d(\omega) = C_g(\omega)\frac{\Delta t(\omega)}{2} \tag{37}$$

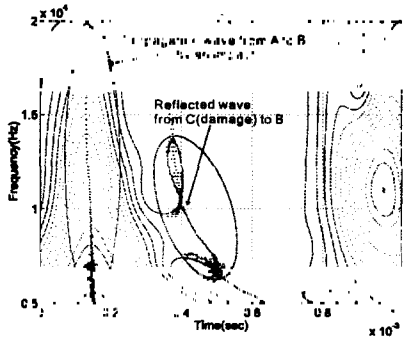

(a) The normalized scalogram

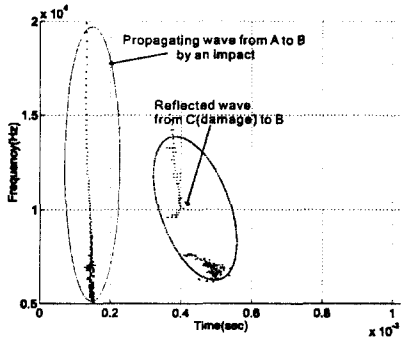

(b) The corresponding ridges of the strain signal measured at B in a beam shown in Fig. 1.

Figure 6: With $G_s = 5.0$.

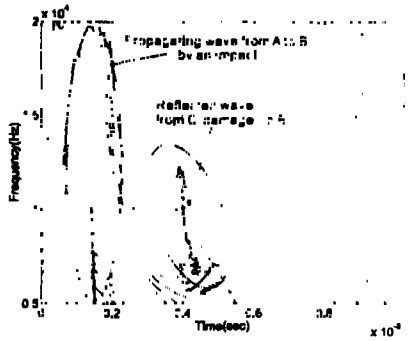

(a) The normalized scalogram

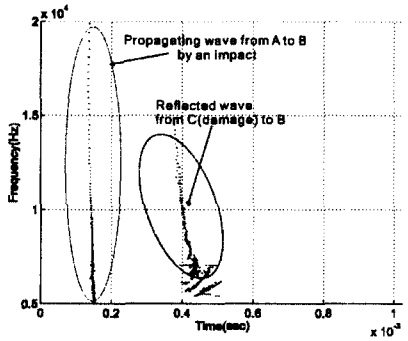

(b) The corresponding ridges of the strain signal measured at B in a beam shown in Fig. 1.

Figure 7: With $G_s = 3.5$.

where Δt is the difference between the arrival times of the propagating wave from A and the first reflected wave. Though d must be independent of frequency, there always exists the scattering of d over frequencies.

The RMS (root-mean-square) value of the estimated distance in Fig. 8 is averaged over the frequency range between 7 kHz and 12 kHz. As expected, the use of $G_s = 3.5$ yields a better estimation of the distance between B and C. It is worth noting that scattering near the low frequency in Fig. 8 (a) is quite severe. This is because not all the conditions stated by Eqs. (36) are satisfied with $G_s = 5.0$ in this frequency range: see Fig. 3.

3. CONCLUSIONS

In this paper, we investigated theoretically why the wavelet transform outperforms the short-time Fourier transform for the analysis of some wave signals. Specifically, the role of CWT in the analysis of waves signal where instantaneous frequencies change rapidly was addressed. The theoretical analysis using the experimentally measured wave signals indeed confirmed the validity of the present investigation.

REFERENCES

[1] **Mallat, S.**, "A Wavelet Tour of Signal Processing", Academic Press, New York, 1998.

[2] **Kim, Y. Y.** and **Kim, E.-H.**, *"A New Damage Detection Method Based on a Wavelet Transform"*, *IMAC 18th*, 2000.

[3] **Delprat, N. Escudié, B. G. P. K.-M. R. T. P.** and **Torrésani, B.**, *"Asymtotic Wavelet and Gabor Analysis: Extraction of Instantaneous Frequencies"*, IEEE Trans. on Information Theory, Vol. 38, No. 2, 1992.

[4] **Doyle, J. F.**, "Wave Propagation in Structures", Springer-Verlag, New York, 2nd edn., 1997.

[5] **Kishimoto, K. Inoue, H. H. M.** and **Shibuya, T.**, *"Time Frequency Analysis of Dispersive Waves by Means of Wavelet Transform"*, ASME trans. J. of Applied Mechanics, Vol. 62, 1995.

[6] **Inoue, H. Kishimoto, K.** and **Shibuya, T.**, *"Experimental Wavelet Analysis of Flexural Waves in Beams"*, Experimental Mechanics, Vol. 36, No. 3, 1996.

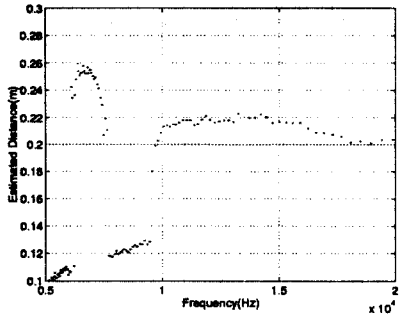

(a) With $G_s = 5.0$.

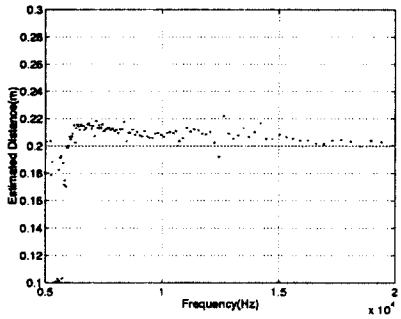

(b) With $G_s = 3.5$.

Figure 8: Estimated distance from the measurement location B to the damage location using the ridges of the normalized scalogram.